Lattice and Valence Electronic Structures of Crystalline Octahedral Molybdenum Halide Clusters-Based Compounds, Cs2[Mo6X14] (X = Cl, Br, I), Studied by Density Functional Theory Calculations

Norio Saito, Stéphane Cordier, Pierric Lemoine, Takeo Ohsawa, Yoshiki Wada, Fabien Grasset, Jeffrey S. Cross, Naoki Ohashi

Lattice and Valence Electronic Structures of Crystalline Octahedral Molybdenum Halide Clusters-based Compounds, $Cs_2[Mo_6X_{14}]$ (X = Cl, Br, I), Studied by Density Functional Theory Calculations

Norio Saito[a,b,e], Stéphane Cordier[d], Pierric Lemoine[d], Takeo Ohsawa[b,c], Yoshiki Wada[b,e], Fabien Grasset[b,e], Jeffrey S. Cross[a], and Naoki Ohashi[b,c,f,*]

[a]*Department of Metallurgy and Ceramics Science, Tokyo Institute of Technology (Tokyo Tech.), 2-12-1 Ookayama, Meguro, Tokyo 152-8551, Japan*

[b]*National Institute for Materials Science (NIMS), 1-1 Namiki, Tsukuba, Ibaraki 305-0044, Japan*

[c]*NIMS-Saint-Gobain Center of Excellence for Advanced Materials, NIMS, 1-1 Namiki, Tsukuba, Ibaraki 305-0044, Japan*

[d]*Institut des Sciences Chimiques de Rennes (ISCR UMR 6226), University of Rennes 1 (UR1), General Leclerc, Rennes 35042, France*

[e]*Laboratory for Innovative Key Materials and Structures (LINK UMI 3629), NIMS, 1-1 Namiki, Tsukuba, Ibaraki 305-0044, Japan*

[f]*Materials Research Center for Element Strategy (MCES), Tokyo Tech., 4259 Nagatsuta, Midori-ku, Yokohama 226-8503, Japan*

Abstract

The electronic and crystal structures of $Cs_2[Mo_6X_{14}]$ (X = Cl, Br, I) cluster-based compounds were investigated by density functional theory (DFT) simulations and experimental methods such as powder X-ray diffraction (XRD), ultraviolet-visible (UV-Vis) spectroscopy, and X-ray photoemission spectroscopy (XPS). The experimentally determined lattice parameters were in good agreement with theoretically optimized ones, indicating the usefulness of DFT calculations for the structural investigation of these clusters. The calculated band gaps of these compounds reproduced those experimentally determined by UV-Vis reflectance within an error of a few tenths of an eV. Core-level XPS and effective charge analyses indicated bonding states of the halogens changed according to their sites. The XPS valence spectra were fairly well reproduced by simulations based on the projected electron density of states (PDOS) weighted with cross-sections of Al K_α, suggesting that DFT calculations can predict the electronic properties of metal-cluster-based crystals with good accuracy.

Keywords: octahedral cluster; molybdenum halide; DFT calculation; XPS; electronic structure

Introduction

Octahedral metal cluster complexes, $[M_6L^i_8L^a_6]^{n-}$ (M = Mo, W, or Re; L^i = inner ligand; L^a = apical ligand), have attracted much attention, being regarded as building blocks for the construction of unique solid state inorganic and hybrid organic/inorganic compounds[1,2] and nanostructures[3,4] exhibiting interesting chemical and physical properties.[5] As the size of these complexes is much larger than that of mononuclear ones, they can crystallize with various large inorganic (e.g., Cs^+) and molecular organic counter cations.[5] Indeed, the combination of these metal cluster complexes and organic molecules enables the design of numerous functional structures, such as meso-scale structured materials[6] and highly dimensional supramolecular assemblies.[7]

An interesting feature of such metal-cluster-based compounds is the tunability of their properties by choosing an appropriate combination of M, L^i, and L^a [8–11] or by crystallization with various counter cations.[12] For example, some of these compounds show electric conductivity or superconductivity,[13,14] while those with a relatively large band gap energy (E_g) show useful luminescence,[15–17] photocatalytic,[18–20] and redox properties.[21] Numerous studies on nanostructure synthesis have been conducted to enhance the useful functions of these cluster compounds.[22–27] In particular, $[Mo_6X^i_8X^a_6]^{2-}$ (X = Cl, Br, I) complexes have been widely studied because of their broadband red luminescence under UV or blue light illumination.[28] Highly efficient phosphors emitting red light under excitation with blue light-emitting diodes (LEDs) are very important in solid-state lighting devices. Hence, the optimization of chemical compositions and structures of these compounds is promising for their applications as phosphors. In fact Kitamura and his

related group have developed novel metal-cluster-based compounds with high luminescence efficiency through modification of cluster's chemical composition.[29,30]

An effective exploration strategy of these complex systems involves the utilization of theoretically predicted composition-structure-property relationships. One of the earlier studies on the molecular orbital (MO) calculation of $[Mo_6Cl_{14}]^{2-}$ cluster was reported by Cotton in 1978.[31] After that electronic properties of the metal cluster complexes such as chemical state and absorption energy have been calculated everywhere since 1990.[32–36] However, most of those studies were based on MO calculations, where neither the presence of counter cations nor lattice periodicity were considered and electronic structures of spatially isolated and electrically charged metal cluster complexes were calculated, although it is reasonable to expect that exchange of counter cations should cause changes in atomic arrangements and effective charge of the complexes. Hence, in order to investigate electronic structure and structural stability of the metal-cluster-based compounds in crystalline form, it is necessary to perform electronic structure calculations based on crystalline periodicity with charge neutrality. Furthermore, most of those calculations were performed using classical functionals, such as the Hartree-Fock approximation. Thus, the utilization of updated density functional theory (DFT), e.g., the generalized gradient approximation (GGA),[37] and consideration of lattice periodicity including counter cations is needed for more accurate predictions of composition-structure-property relationships in metal cluster complexes.

In this context, we have recently studied the crystal structure of $Cs_2[Mo_6Cl_{14}]$[38] using plane-wave-based DFT calculations to examine the applicability of DFT for reproducing the structural and electronic features of metal-cluster-based crystalline compounds. As a result, it was shown

that the accuracy of conventional DFT is sufficient to predict formation energy differences between polymorphs of crystalline $Cs_2[Mo_6Cl_{14}]$, implying that DFT calculations can be a useful tool for exploring metal-cluster-complex-based solid systems. Hence, we have attempted to predict the optical properties of metal-cluster-based compounds using updated DFT calculations.

This study describes DFT calculations on $Cs_2[Mo_6X_{14}]$ (X = Cl, Br, I), aiming to accurately reproduce the effects of halogen substitution using the GGA functional. To examine the consistency between experimental observations and theoretical predictions, the observed lattice parameters were compared with the theoretically optimized ones. Furthermore, the reproducibility of theoretically predicted electronic structures was examined by comparison with experimentally observed X-ray photoemission (XPS) spectra and E_g values.

Materials and methods

Sample preparation

The metal cluster-based solid state ternary halides $Cs_2[Mo_6X_{14}]$ (X = Cl, Br, I) were synthesized and purified using procedures reported elsewhere.[38–40] After purification, all samples were heated at 150 °C for 1 h in a glove box filled with dry N_2 gas (< 0.1 ppm H_2O). In our previous study,[38,39] expansion of lattice parameters of $Cs_2[Mo_6Cl_{14}]$ due to insertion of water molecules from environmental humidity was detected and those inserted water molecules could be removed by heat treatment in dry ambient at 150 °C. Hence, similar dehydration treatment was performed to all the samples prepared in this study to observe intrinsic nature of pure $Cs_2[Mo_6X_{14}]$ without influence of water molecule insertion.

Characterization and analyses

The crystal structures of the obtained powders were characterized by XRD using a RINT-Ultima III diffractometer (Rigaku Co. Ltd., Tokyo, Japan) with monochromatic Cu K_α radiation (λ = 0.15418 nm). The observed diffraction patterns were indexed assuming that the samples crystallized in the trigonal centrosymmetric $P\bar{3}1c$ space group.[38–40] Finally, the lattice parameters of $Cs_2[Mo_6X_{14}]$ were refined using the method of least squares.

The diffuse reflectance spectra of $Cs_2[Mo_6X_{14}]$ in the near-UV to near-infrared (near-IR) range were measured using a SolidSpec-3700 spectrophotometer (Shimadzu Corp., Tokyo, Japan) equipped with a $BaSO_4$ integrating sphere. Both core-level and valence band range XPS spectra of samples were obtained using a Σ-probe spectrometer (Thermo Fisher Scientific K.K, Yokohama, Japan) equipped with a monochromated Al K_α X-ray source (hv = 1486.6 eV). The pass energy was set at 20.0 eV for all spectra, with the instrumental resolution of electron energy being ~0.2 eV. Samples were attached on an adhesive tape containing carbon particles. When obvious charging under X-ray irradiation occurred, a charge neutralizer employing both Ar^+ ion and electron emitters was used to eliminate charging. All binding energies were calibrated with respect to the C 1*s* peak of adventitious carbon at 284.6 eV. After subtraction of the spectral background using Shirley's method,[41] the observed spectra were fitted by mixed Gaussian-Lorentzian functions using the method of least squares to calculate the integrated peak intensities and relative shifts of peak positions.

Computational methods

All DFT calculations were performed for the trigonal form of $Cs_2[Mo_6X_{14}]$ (X = Cl, Br, I), which belongs to the $P\bar{3}1c$ centrosymmetric space group,[38–40] as shown in Fig. 1(a), with

structural optimizations performed by applying structural constraints to maintain $P\bar{3}1c$ symmetry. It should be noted that this simplified model was not perfectly compatible with the experimentally refined crystal structure of $Cs_2[Mo_6Br_{14}]$.[40] Indeed, as shown in Fig. 1(b), the XRD characterization of $Cs_2[Mo_6Br_{14}]$ indicated splitting of Cs sites along the *c*-axis and the presence of interstitial Cs sites at (0, 0, 0.25) with a 12% occupancy.[40] However, the simplified model shown in Fig. 1(a) was adopted for DFT calculations of all $Cs_2[Mo_6X_{14}]$ complexes (including $Cs_2[Mo_6Br_{14}]$) due to limited computational resources. The structural parameters used to construct the initial structural model are listed in Table S1.

All DFT calculations were performed with the CASTEP code[42] utilizing the plane wave pseudo-potential method.[43] The norm-conserving pseudo-potentials (NCPPs)[44] were generated using the OPIUM code.[45,46] The revised Perdew-Burke-Ernzerhof GGA functional for solid-state compounds (PBEsol)[47] was employed for energy minimization using the Pulay density mixing scheme.[48] The cell parameters and atomic coordinates were relaxed using a quasi-Newton method and the Broyden-Fletcher-Goldfarb-Shanno Hessian update scheme.[49] Electron spin polarization was considered for all DFT calculations. The plane wave cut-off energy was set to 830 eV, a Monkhorst-Pack grid[50,51] (4 × 4 × 3 mesh) was employed for Brillouin zone sampling, and a 96 × 96 × 144 mesh was adopted for the fast Fourier transformation. The convergence tolerances were set to 5×10^{-5} nm for atomic displacement, 5×10^{-6} eV/atom for total energy, 0.1 eV/nm for maximum interatomic force, and 0.02 GPa for pressure. The effective charges of constituent elements were estimated using two methods, i.e., Mulliken[52,53] and Hirshfeld population analyses.[54,55]

To compare the observed spectra with calculated results, additional simulations of optical and electronic spectra were performed. Optical absorption spectra were simulated by computing inter-band transition probabilities using the results of DFT calculations. The number of *k*-points involved in the simulation of optical properties was set to 21 per irreducible Brillouin zone. Valence band XPS spectra were also simulated by assuming a previously reported photoionization probability.[56]

Results and discussion

Structural analyses

The observed XRD patterns shown in Fig. 2 were identified to be the trigonal phase as previously reported in references.[38–40] However, for the sample with X = Cl, some peaks (denoted by arrows in Fig. 2), not assignable to $Cs_2[Mo_6Cl_{14}]$, were found. As previously reported,[38] these extra peaks were from the secondary phase(s) crystallizing during synthesis and/or purification. The secondary phase was assigned to be $Cs_2[Mo_6Cl_{14}].H_2O$ as reported in a separate report.[39] As the fraction of this secondary phase in the currently prepared sample should be negligibly small, we assume that the obtained results represent the characteristics of the trigonal $Cs_2[Mo_6Cl_{14}]$ phase. The refined lattice parameters of each sample, listed in Table 1, were almost identical to those reported in literature,[38–40] being only slightly smaller. This deviation was attributed to the removal of volatile impurities, such as water related molecules. We previously reported that insertion of water molecules from ambient condition into the trigonal lattice of $Cs_2[Mo_6Cl_{14}]$ caused slight expansion of the lattice volume, and the water impurities could be removed by heating in an atmosphere of dry N_2, along with contraction of lattice volume.[38] Hence, the samples prepared in this study are assumed to be very close to their intrinsic states.

The results of structural optimization and energy minimization converged well for all calculations, with the optimized lattice parameters being close to experimental values, as listed in Table 1. The calculated lattice parameters were well-matched with the experimental ones along the *a*-axis, being somewhat longer along the *c*-axis. We note that the overestimation of lattice parameters is due to a general tendency of the GGA functional.[57] The detailed optimized lattice structures and fractional positions of all atoms in the lattice are summarized in Table S2 in the Supporting Information. These parameters are also consistent with the values reported in literature,[38,40] indicating that the DFT structural optimization was successful, and the lattice structures were consistently reproduced by DFT calculations employing the PBEsol functional.

Electronic structures

The valence band structure of $Cs_2[Mo_6X_{14}]$ varied with X, as seen from the PDOS of $Cs_2[Mo_6X_{14}]$ (Fig. 3) obtained using the PBEsol functional after structural optimization. As up-spin and down-spin orbitals were identical, this figure shows the total PDOS profiles, featuring a summation of up- and down-spin orbitals. As can be seen, the Mo 4*d* states were dominantly found around the valence band maximum (VBM), while the valence *p*-orbitals of X were distributed in the relatively deeper parts of the valence band. In particular, the valence *p*-states of X^is were located in deeper parts of the valence band compared to those of X^as. Moreover, the *s*-orbitals of X in the semi-core region (> 9 eV) showed similar behavior: the *s* states of X^is were deeper than those of X^as. These results indicate that the chemical states of X^as and X^is are obviously different. In addition, the energy dispersion of valence electrons also varied with X. For instance, the energy dispersion of the valence *p*-orbitals of X^as obviously changed with X

(Fig. 3). Indeed, the population of X *p*-orbitals within VBM increased with the atomic number of X. Moreover, the dispersion of valence X *p*-orbitals seemed being broader with the increase of the atomic number of X. These valence band structure changes are reflected in the results of charge analyses shown in Table S3. The charge of X became more positive with increasing atomic number, mirrored by the charge of Mo becoming more negative. These results indicate that Mo–X bonds are highly ionic for X = Cl and less ionic for X = Br and I. Although the results of charge analyses suggest changes in chemical bonds between Mo and X, the calculated charge values seem to be inconsistent from the viewpoint of experimental chemistry. Namely, the positively charged X and negatively charged Mo atoms do not correspond to the intuitively expected results, since Mo and X are usually considered as a cation and anions, respectively. Such inconsistencies between intuitive and calculated results might be due to the charge analysis methodology adopted in this study, implying that the PDOS obtained by projection of the total electron distribution to the assumed atomic orbitals should feature a similar problem. Considering the difficulties in evaluating reasonable effective charges,[58] the characteristics of Mo–X bonds are discussed below in terms of real-space orbital population distribution.

Figure 4 shows the highest occupied molecular orbital (HOMO) of $Cs_2[Mo_6X_{14}]$. For X = I, the HOMO was dominated by Mo 4*d* and I 5*p* states at X^a sites (I^a-5*p*). On the other hand, for X = Cl and Br, the HOMO featured contributions from the *p*-states of X^i. In particular, the HOMO of $Cs_2[Mo_6Cl_{14}]$ was dominated by Mo 4*d* and Cl 3*p* states at X^i (Cl^i-3*p*). Note that the HOMO of $Cs_2[Mo_6Br_{14}]$ was intermediate between that of $Cs_2[Mo_6Cl_{14}]$ and $Cs_2[Mo_6I_{14}]$. These results indicate that the electronic structure of the valence band (VB) of $Cs_2[Mo_6X_{14}]$ obviously changes with X despite the structural similarity.

The valence band structures of $Cs_2[Mo_6Cl_{14}]$ and $Cs_2[Mo_6I_{14}]$ are shown in Fig. 5 to investigate the effect of X in $Cs_2[Mo_6X_{14}]$. As seen in this figure, the electronic bands within the VB are classified into bundles. As the electronic states of every cluster are highly localized, every band possesses a small dispersion in *k*-space, which is the reason behind the formation of bundles. Thus, the observed electronic structure resembles the energy levels of isolated molecules. As seen from Fig. 5, the energetic order of the bundles was fairly independent of X; for instance, *Φ*D and *Φ*E of $Cs_2[Mo_6I_{14}]$ resembled *Φ*4 and *Φ*5 of $Cs_2[Mo_6Cl_{14}]$, respectively. However, the number of bands in the *Φ*A–*Φ*E bundles in $Cs_2[Mo_6I_{14}]$ and that of *Φ*1–*Φ*5 in $Cs_2[Mo_6Cl_{14}]$ equaled 28 and 22, respectively, implying that several bands located above *Φ*E in $Cs_2[Mo_6I_{14}]$ had energies below that of *Φ*5 in $Cs_2[Mo_6Cl_{14}]$. Indeed, *Φ*F and *Φ*6 show different numbers of bands and dissimilar energy dispersions. Another typical difference between $Cs_2[Mo_6Cl_{14}]$ and $Cs_2[Mo_6I_{14}]$ can be found in bundles located relatively deep in the valence band. Both *Φ*14 and *Φ*O bundles are close to the bottom of the valence band and consist of 12 electron bands. However, the energy dispersion of *Φ*14 is obvioulsly narrower than that of *Φ*O.

Differences in the electronic band structure of $Cs_2[Mo_6Cl_{14}]$ and $Cs_2[Mo_6I_{14}]$ are likely due to the variable degree of Mo-X hybridization. Since Fig. 5 indicates that the energy dispersion of all bundles was wider for $Cs_2[Mo_6I_{14}]$ than for $Cs_2[Mo_6Cl_{14}]$, the electrons in $Cs_2[Mo_6Cl_{14}]$ are presumably more strongly localized than those in $Cs_2[Mo_6I_{14}]$. This understanding is consistent with the variation of orbital shapes shown in Fig. 6. The wave functions in $Cs_2[Mo_6Cl_{14}]$ are highly localized on all atoms, and the Mo–Cl bonds seem to be highly ionic. In support of this, the valence orbital overlap of Cl and Mo is negligibly small, as shown by the iso-surfaces of

electron orbitals. In contrast, the electron orbitals in $Cs_2[Mo_6I_{14}]$ show covalent bond character. For instance, the electron orbital involved in *Φ*O is located at the center of the Mo–I bond, and all orbital distributions are not homogeneous, but rather anisotropic, as seen in *Φ*J, *Φ*K, and *Φ*M. Another characteristic feature found in $Cs_2[Mo_6I_{14}]$ is the hybridization of I^i and I^a, as exemplified by *Φ*K. The difference between *Φ*14 and *Φ*O is also interesting. As mentioned above, *Φ*14 showed a very narrow energy dispersion compared to that of *Φ*O. Typical orbital distributions of bands involved in *Φ*14 and *Φ*O are compared in Figs. 6(o) and (p). All Cl^i atoms contribute nearly equally to every electron orbital in *Φ*14, while the contribution of I^i atoms to electron orbitals of *Φ*O differ from each other. This is an indication that the electron orbitals of $Cs_2[Mo_6I_{14}]$ possess a strong directionality, which is characteristic of covalent bonds. Indeed, the calculated total electron density in $Cs_2[Mo_6Cl_{14}]$ showed a spherical distribution centered at every Cl, while that in $Cs_2[Mo_6I_{14}]$ was distorted from spherical shape (Fig. S1). Hence, it was concluded that Mo–X bonds become more covalent with increasing halogen atomic number.

Reproducibility of typical electronic spectra

Figure 7 compares calculated and observed optical absorption spectra. Herein, experimental spectra were obtained from the observed diffuse reflectance shown in Fig. S2 using the KM function.[59,60] The calculated spectra were obtained by applying Gaussian broadening with 0.05 eV in width. The observed and calculated absorption edges agreed within an error of less than 0.2 eV, indicating that the calculated E_g well reproduced the experimental values. It has been suggested that E_g calculated by conventional DFT methods tends to be smaller than the experimentally obtained values.[61,62] However, for this system, the calculated E_g showed good agreement with experimental observations. It should be also noted that the HOMO-LUMO gaps evaluated in the other study employing a molecular orbital method were much wider than the

experimental values of E_g. For instance, the HOMO-LUMO gap for X= Cl evaluated by the molecular orbital calculation was reported to be 3.3 eV in the reference.[63] The comparison of present results with experimental results and the other reported calculations indicates that the corresponding energy band structure calculations based on DFT are appropriate for predicting band gap energies in $Cs_2[Mo_6X_{14}]$ systems.

It has to be reminded that we have employed energy band structure calculation involving lattice periodicity. The most definite difference between the previous studies[31–36] using the cluster calculation based on molecular orbital concept and present study is that present one dealt with neutral lattice with crystalline periodicity. As this study is based on crystalline lattice, effective charge of the metal cluster complex and counter cation, i.e., Cs, varied with chemical compositions as described above. Hence the effective charge of the metal cluster complexes could be converged into reasonable values. We suppose that this is the most significant merit of this study where the lattice periodicity has been considered. Indeed the accordance between experimental and calculated absorption spectra is good news for researchers investigating the electric and optical properties of metal-cluster-based compounds, since DFT simulation based on lattice periodicity is useful for material design, e.g., obtaining compounds with the desired E_g by substitution of X by another halogen (X') to form $Cs_2[Mo_6(X, X')_{14}]$. Namely, we can expect that prediction of the stable structure and physical properties of metal complex compound with various counter cation is possible with plane wave DFT calculations based on lattice periodicity.

The observed XPS core-level spectra of $Cs_2[Mo_6X_{14}]$ are shown in Fig. 8. The core-level spectra of halogens featured two doublets, denoted P_1 and P_2. Since these doublets originated from spin-orbit coupling, profile fitting was performed assuming the presence of two different halogen species. Indeed, the presence of two halogen ion components in XPS spectra has been

reported,[64–66] with these two peaks attributed to X^a and X^i. The results of peak fitting are summarized in Table 2. The integrated intensity ratio of P_1 and P_2 (S_1/S_2) ranged from 0.74 to 0.77, consistently corresponding to 0.75 (= 6/8), which is reasonably attributed to X^a and X^i in the $[Mo_6X^i_8X^a_6]^{2-}$ complex. The energy difference between P_1 and P_2 ($E_{b2} - E_{b1}$) equaled 2.1 eV for X = Cl and Br, being equal to 1.6 eV for X = I. As the current DFT study used pseudo-potential and not all-electron calculations, it was not possible to determine the orbital energies of the observed core levels. On the other hand, the above experimentally observed energy difference is comparable to the energy difference of semi-core states calculated by DFT. Based on the calculated DOS shown in Fig. 3, the values of $E_{b2} - E_{b1}$ estimated by DFT simulations equaled 2.1 eV for X = Cl, 2.0 eV for X = Br, and 1.7 eV for X = I. These estimated values were in agreement with the experimental ones within an error of 0.1 eV, providing further evidence that the results of DFT calculations were consistent with experimental observations. The results of the corresponding XPS studies also indicate that the variation of the electronic structure of $Cs_2[Mo_6X_{14}]$ with X discussed above was a reasonable consideration. As displayed in Fig. 6(l), electron orbitals with contributions from *p*-orbitals of both I^i and I^a were found in the results of the DFT study on $Cs_2[Mo_6I_{14}]$. This indicates that the relatively small energy separation between the levels originating from I^i and I^a resulted in hybridization between I^i and I^a.

Here, it should be noted that the variation of ionicity of halogen at X^a and X^i site indicated by DFT calculation enables us to explain observed reactivity of the metal cluster complexes. From the viewpoint of chemical reaction for elimination and exchange of halogens in the metal-cluster-based compounds, halogen at X^a site in the complex with X^i = Cl or Br can be replaced by other halogens,[67,68] but halogen substitution in $[Mo_6I_{14}]$-complex seems to be difficult. As the complex with X = Cl and Br possesses relatively strong ionicity as indicated by DFT calculation,

substitution of X^a site in $[Mo_6Cl_{14}]$- and $[Mo_6Br_{14}]$-complex should be allowed when the electric charge of X^a site is maintained. However, replacement of I at X^a site by other halogen is expected to be limited because relatively high electronegativity of Cl and Br is not compatible to covalent bond formed in $[Mo_6I_{14}]$-complex. Hence, we can conclude that DFT calculation which visualize characteristics of chemical bonds is very useful tool for understanding of the chemical reactivity of the metal cluster complex compounds.

In addition to core-level XPS, the observed valence band XPS spectra and calculated PDOS were also compared, as shown in Fig. 9. Herein, the calculated XPS spectra were obtained by multiplying the reported photoionization probability listed in Table S4 with the PDOS shown in Fig. 3. Details of the simulation method are described in the Supporting Information. The shape of the valence band spectrum of $Cs_2[Mo_6X_{14}]$ showed an obvious dependence on X, indicating corresponding changes in the electronic band structure of $Cs_2[Mo_6X_{14}]$. Comparison of the observed and calculated spectra indicated that the spectral features in the observed spectra were well reproduced in the calculated ones, although the valence band widths of the former were much wider than those of the latter. Note that the presence of two peaks in the Cs 5*p* region of the observed spectra resulted from spin-orbital coupling, not being an indication of the presence of two different electronic states of Cs. In the observed spectra, the semi-core levels of X^i and X^a were not well resolved for X = Br and I due to the overlap of doublets resulting from spin-orbit coupling. However, it is evident that the energy separation between the semi-core states of Cl observed in the XPS spectrum was well reproduced in the calculated spectrum. Hence, we can safely conclude that the band structure of $Cs_2[Mo_6X_{14}]$ was well reproduced by DFT. Accordingly, the above discussion on valence band electron orbitals obtained by DFT

calculations was meaningful, since the calculation results well reproduced the XPS and optical absorption spectra.

Conclusions

In this study, both experimental and theoretical characterizations were carried out to reveal the electronic structure of cluster-based $Cs_2[Mo_6X_{14}]$ ternary solid state compounds. The calculated structural features (lattice parameters) and optical properties (E_g), as well as the calculated DOS of these compounds were consistent with the experimental results, indicating that DFT simulations are appropriate for reproducing and predicting the above properties. The results of DFT calculations indicated that the electronic structure of $Cs_2[Mo_6X_{14}]$ solids depend on the nature of X, although their crystal structures were fairly independent of the nature of X. The most significant electronic structure change due to the variation of X was found to be the difference in the degree of hybridization of Mo–X bonds.

As the calculated results were in good agreement with experimental observations, the DFT technique is considered appropriate for the prediction of electronic and optical properties of $Cs_2[Mo_6X_{14}]$ systems with various compositions. Hence, DFT can be a useful tool to explore the useful properties exhibited by $Cs_2[Mo_6X^i_8X^a_6]$ with various elemental combinations, such as $Cs_2[Mo_6Cl^i_8I^a_6]$, $Cs_2[Mo_6Br^i_8Cl^a_6]$, etc., where X^i and X^a sites are occupied by different elements.

FIGURES

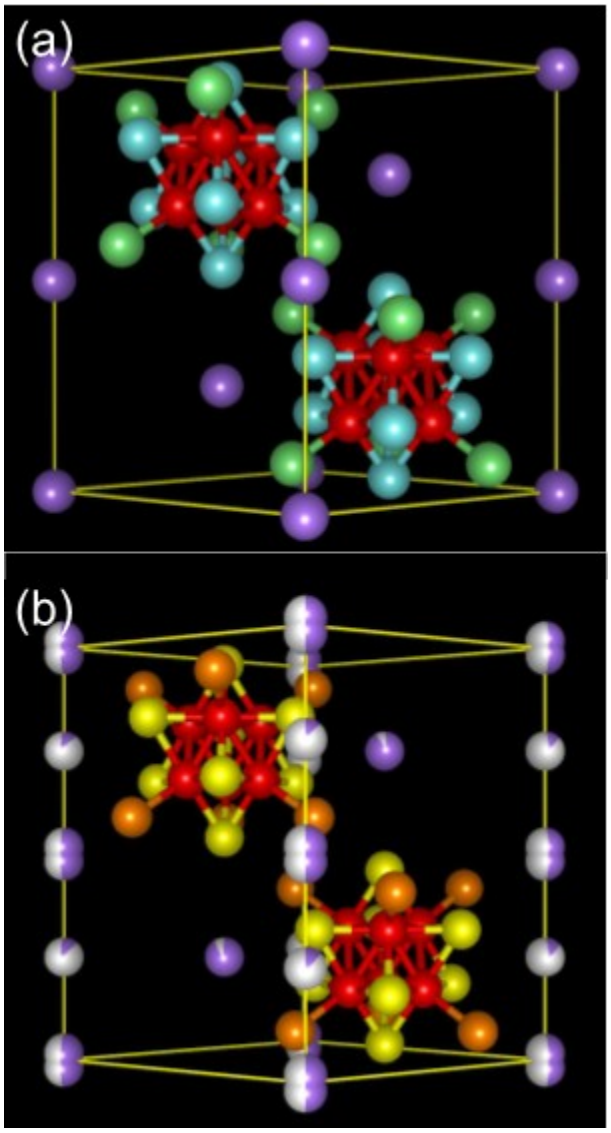

Figure 1. Schematic representation of the crystal structures of trigonal $Cs_2[Mo_6X_{14}]$ belonging to the centrosymmetric $P\bar{3}1c$ space group: (a) X = Cl, I; (b) X = Br. In (b), the additional Cs atom at position 2*a* occupies 12% of the site instead of partially occupying another Cs site at position 2*c*. Furthermore, the other Cs site close to the origin is split into two equivalent sites.

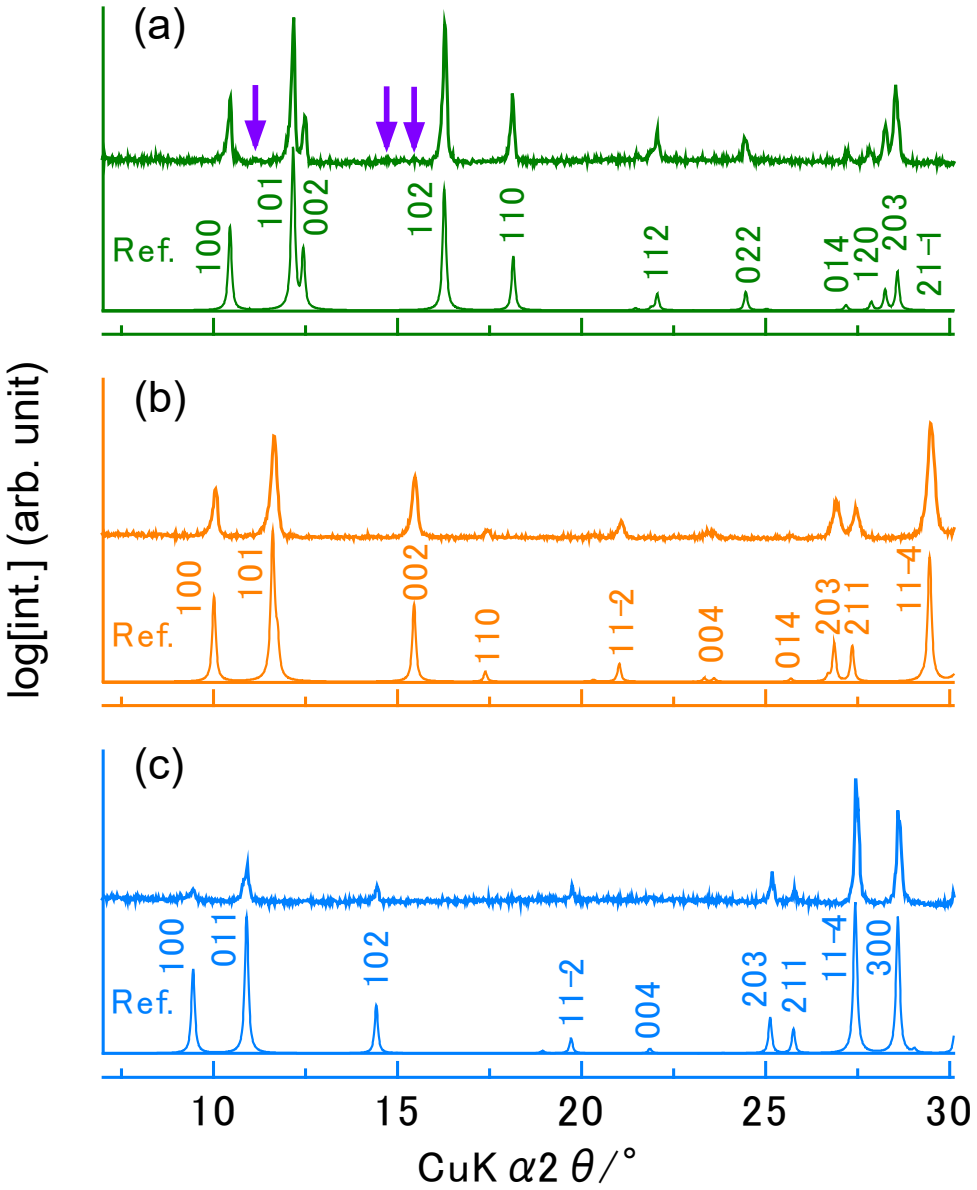

Figure 2. XRD patterns of $Cs_2[Mo_6X_{14}]$: (a) X = Cl, (b) X = Br, and (c) X = I. Arrows denote $Cs_2[Mo_6Cl_{14}].H_2O$.

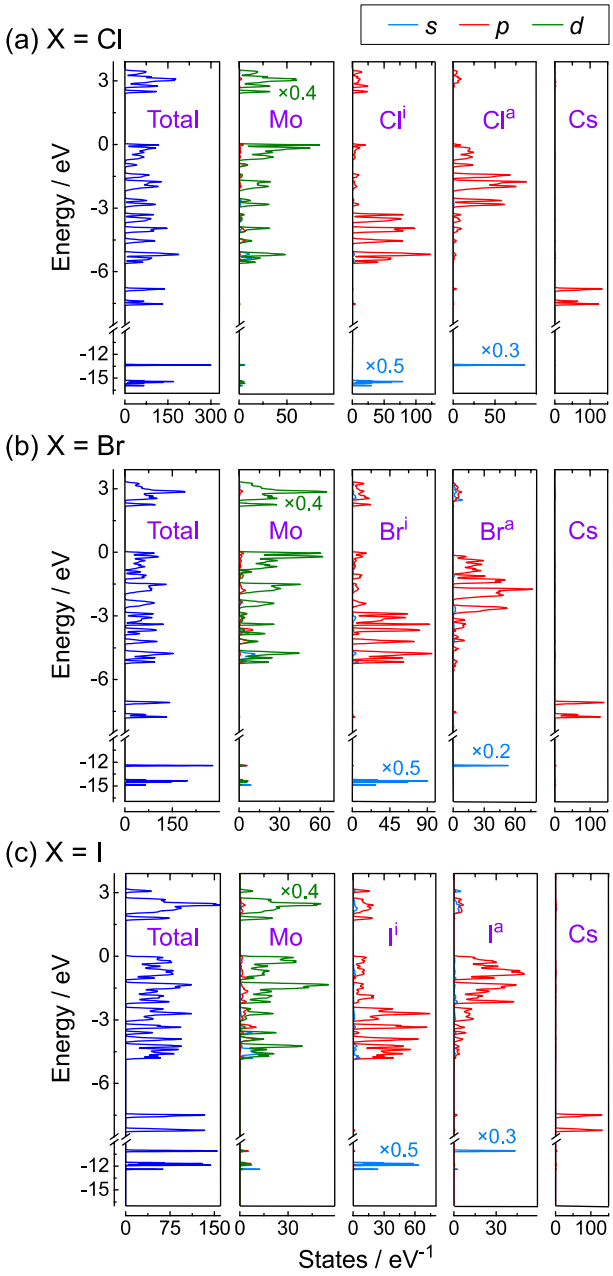

Figure 3. PDOS of $Cs_2[Mo_6X_{14}]$: (a) X = Cl, (b) X = Br, and (c) X = I.

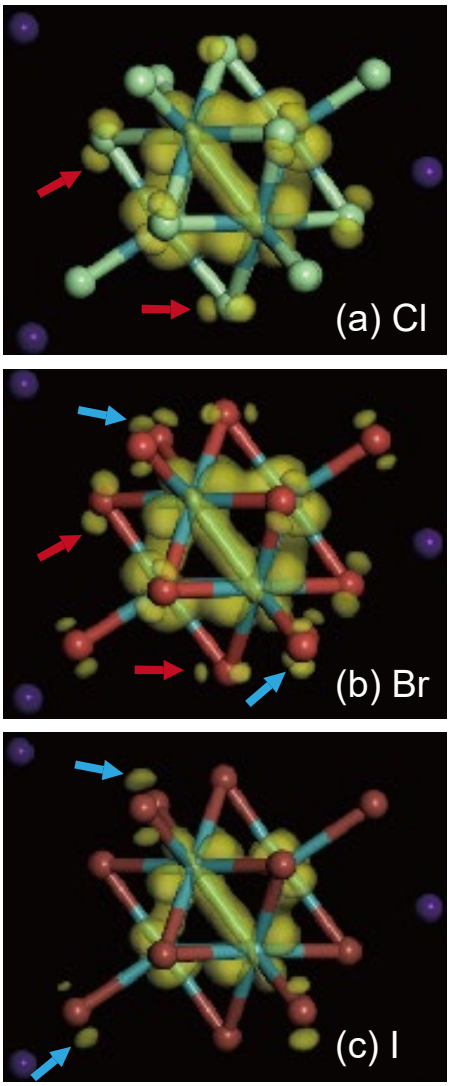

Figure 4. Electron orbital distribution of the highest occupied orbital in $Cs_2[Mo_6X_{14}]$ for (a) X = Cl, (b) X = Br, and (c) X = I. The yellow clouds indicate iso-surfaces normalized at 0.08 $e/Å^3$, and the red and blue arrows indicate the clouds representing the contributions of X^i and X^a, respectively.

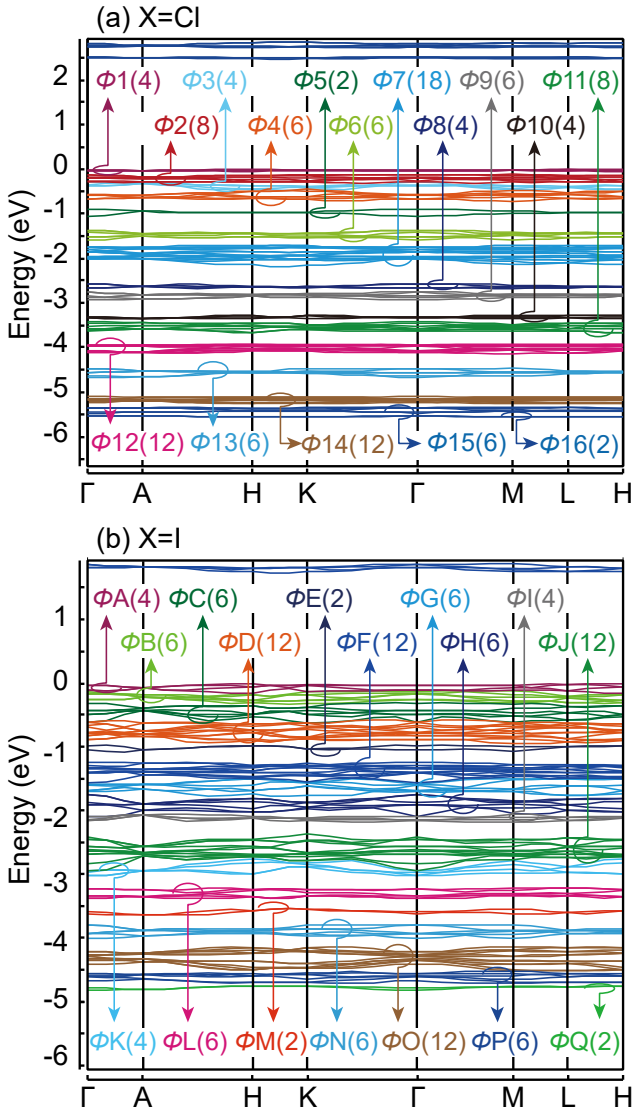

Figure 5. Electron energy band structure of $Cs_2[Mo_6X_{14}]$ in the valence band range for (a) X = Cl, (b) X = I. Every band was classified into bundles, e.g., *Φ*1, *Φ*2, *Φ*3,..., *Φn* for X = Cl and *Φ*A, *Φ*B, *Φ*C, etc. for X = I. The numbers in parentheses show the number of bands involved in every bundle.

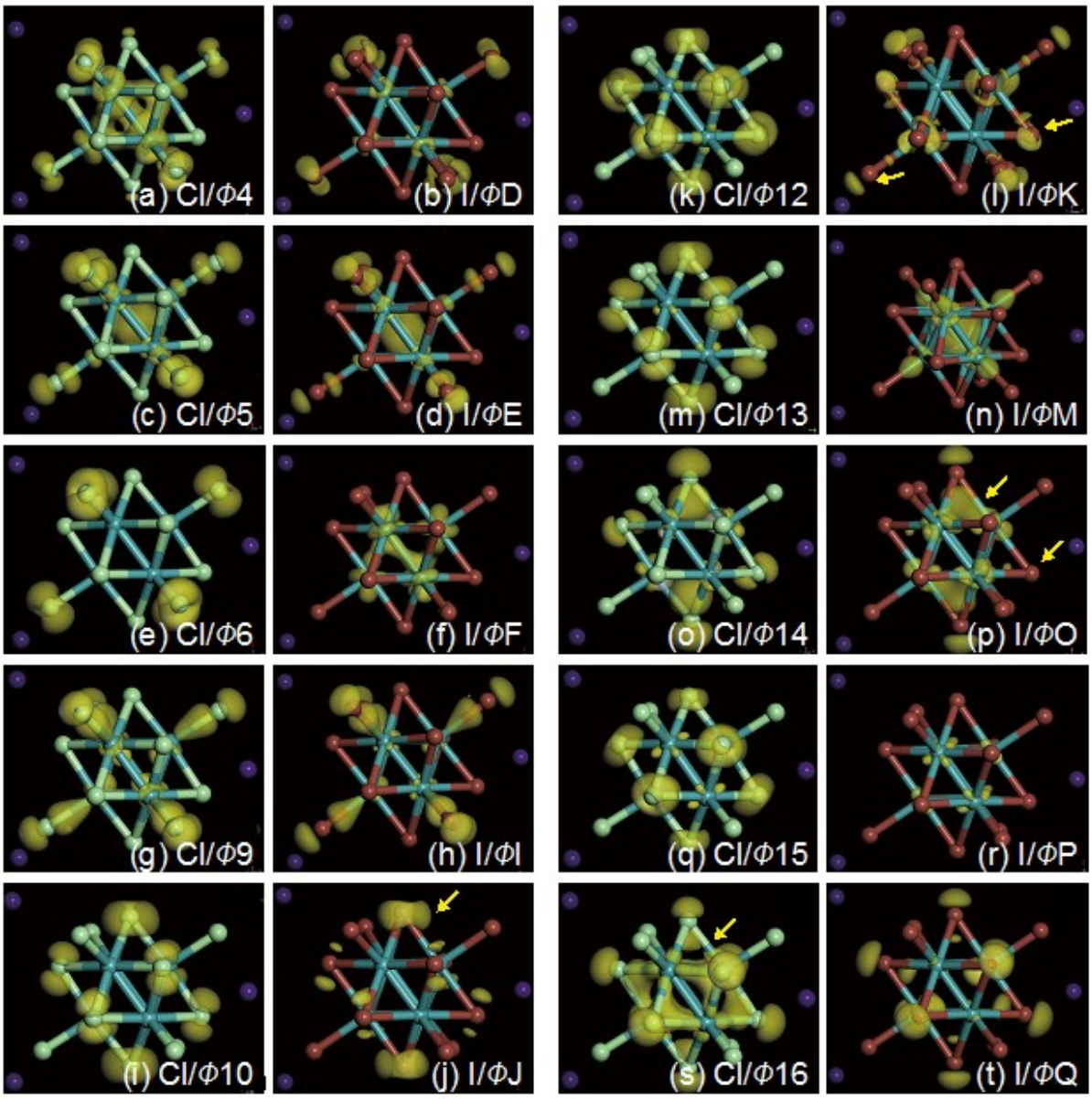

Figure 6. Iso-surface plot of typical electron orbitals in $Cs_2[Mo_6X_{14}]$ for X = Cl and I. The figures (a), (c), (e)…(s) depict representative electronic orbitals of bundles Φ4, Φ5, Φ6,…Φ16 defined in Fig. 5(a) and the figures (b), (d), (f),…(t) exhibit representative electronic orbitals of bundles ΦD, ΦE, ΦF,…ΦQ defined in Fig. 5(b). Arrows indicate characteristic orbital shapes reflecting the chemical states of Mo–X bonds.

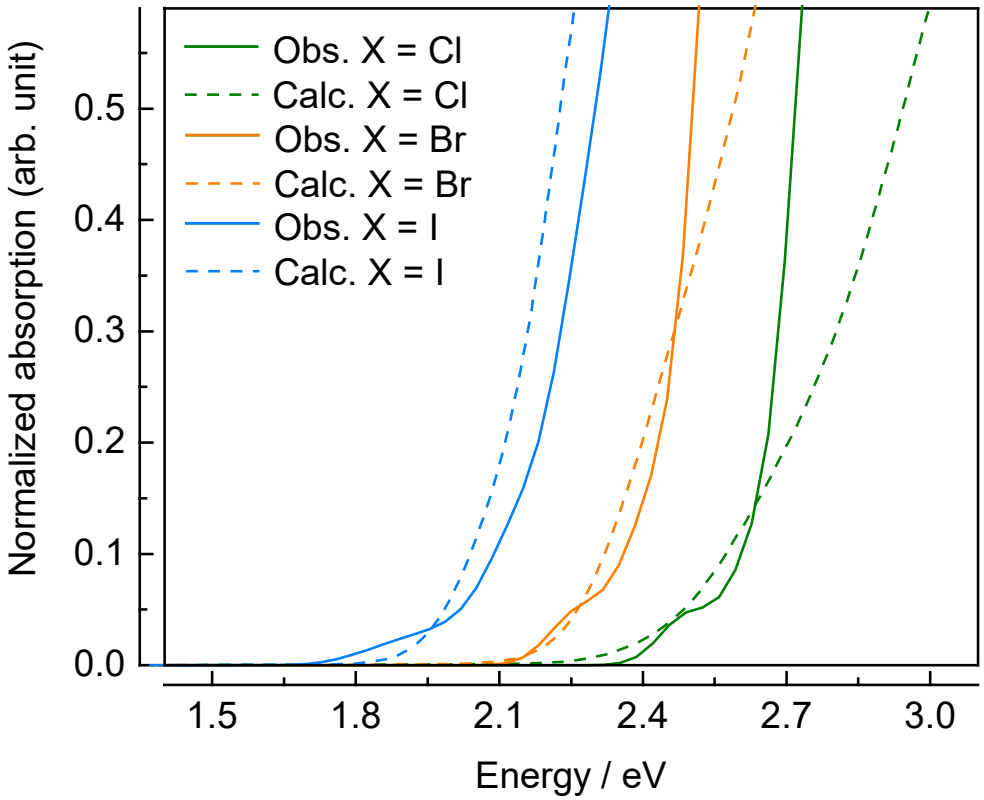

Figure 7. Calculated and observed absorption spectra of $Cs_2[Mo_6X_{14}]$ (X = Cl, Br, I).

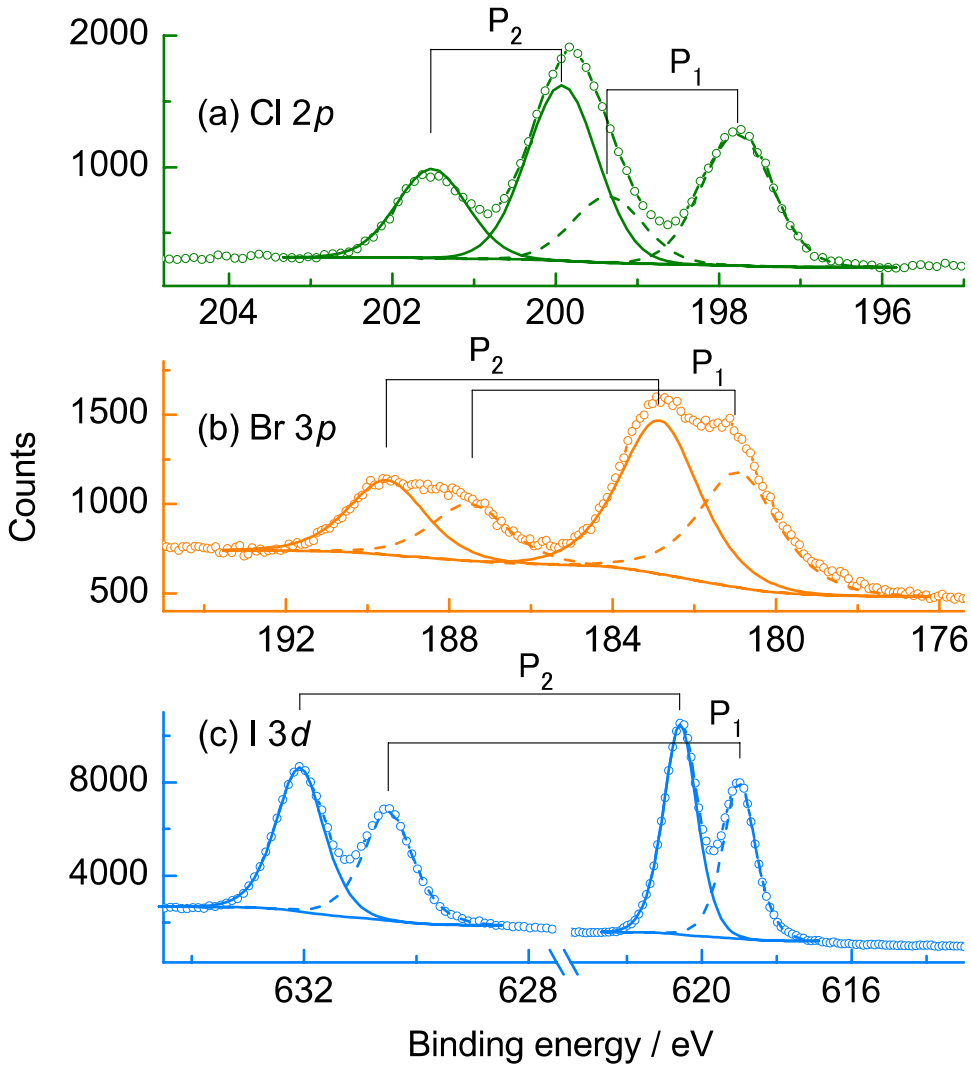

Figure 8. Core-level XPS spectra of $Cs_2[Mo_6X_{14}]$: (a) Cl 2*p* region for X = Cl , (b) Br 3*p* region for X = Br, and (c) I 3*d* region for X = I. P_1 and P_2 indicate the presence of two doublets.

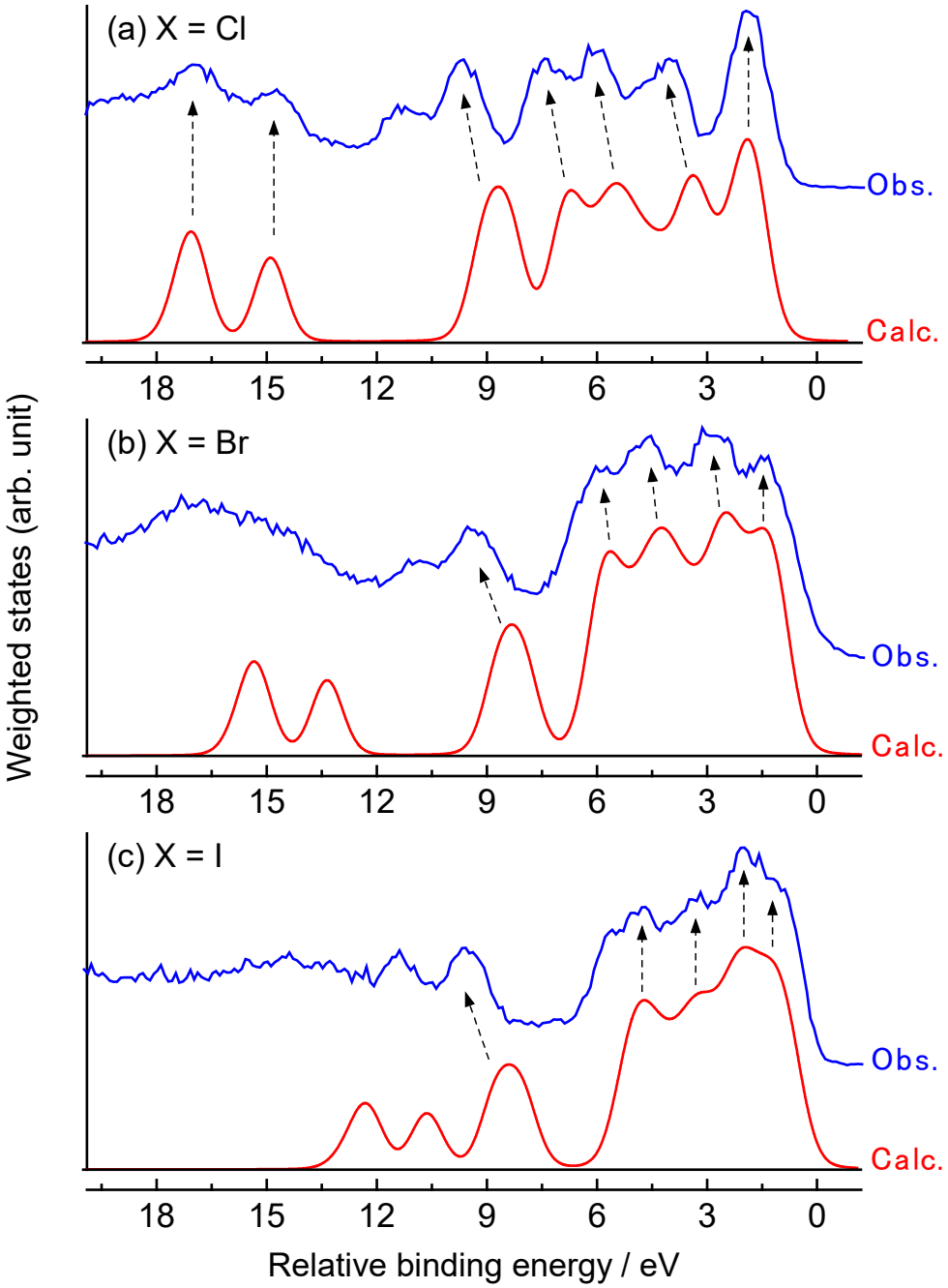

Figure 9. Comparison between the observed and calculated XPS valence spectra of $Cs_2[Mo_6X_{14}]$ for (a) X = Cl, (b) X = Br, and (c) X = I. Arrows denote matching spectral features in the observed and calculated profiles.

Table 1. Refined lattice parameters of trigonal $Cs_2[Mo_6X_{14}]$ (X = Cl, Br, I) in hexagonal expression.

	Lattice parameter		
	a / nm	c / nm	V / nm^3
Experimentally determined in this study			
$Cs_2[Mo_6Cl_{14}]$	0.9789(1)	1.4195(3)	1.1779(1)
$Cs_2[Mo_6Br_{14}]$	1.0156(2)	1.5073(5)	1.3465(2)
$Cs_2[Mo_6I_{14}]$	1.0794(2)	1.6249(5)	1.6394(3)
Calculated in this study			
$Cs_2[Mo_6Cl_{14}]$	0.980	1.475	1.227
$Cs_2[Mo_6Br_{14}]$	1.014	1.550	1.380
$Cs_2[Mo_6I_{14}]$	1.084	1.636	1.665
Indicated in literature [38,40]			
$Cs_2[Mo_6Cl_{14}]$	0.9789(1)	1.4214(2)	1.1796(2)
$Cs_2[Mo_6Br_{14}]$	1.01925(1)	1.50690(3)	1.35574(3)
$Cs_2[Mo_6I_{14}]$	1.0804(5)	1.6258(5)	1.6435(1)

Table 2. Spectral parameters (E_b for peak position and S for relative integrated peak intensity) of halogens in $Cs_2[Mo_6X_{14}]$ (X = Cl, Br, I) obtained by profile fitting under the assumption that all core level profiles comprised two components (P_1 and P_2).

X	Core level	P_1		P_2		$(E_{b2} - E_{b1})$ / eV	S_1/S_2
		E_{b1}/eV	S_1	E_{b2}/eV	S_2		
Cl	2*p* 3/2	197.8	1090	199.9	1460	2.1	0.75
Br	3*p* 3/2	180.8	1730	182.9	2240	2.1	0.77
I	3*d* 5/2	619.0	7790	620.6	10520	1.6	0.74

ASSOCIATED CONTENT

AUTHOR INFORMATION

Corresponding Author

*E-mail: ohashi.naoki@nims.go.jp

Author Contributions

All authors have given their approval to the final version of the manuscript.

Funding Sources

Saint-Gobain company, Centre National de la Recherche Scientifique (CNRS), Université de Rennes 1 and NIMS through the Laboratory for Innovative Key Materials and Structures (LINK *UMI 3629*) with additional contributions from Region Bretagne (France), and Fondation Langlois.

Notes

Any additional relevant notes should be placed here.

Supporting Information Available: Listings of crystal graphic parameters for theoretical calculation studies, the results for the effective charge analyses, contour map of electron density, experimental UV-Vis diffuse reflection data, and photoionization probability data.

ACKNOWLEDGMENT

This work was carried out as part of the France-Japan international collaboration framework (UMI 3629-LINK Center). The authors thank people involved in LINK and related activities,

particularly Dr. David Lechevalier, Dr. Mari Kono, and Dr. Benjamin Dierre of Saint-Gobain KK (Tokyo, Japan), Noée. Dumait, Serge Paofai of ISCR for their contributions to contributions to the synthesis of metal clusters precursors. N.S. would also like to thank Prof. Junzo Tanaka of Tokyo Tech for support and encouragement. The studywas financially supported by Saint-Gobain Company(France), CNRS, Université de Rennes 1 and NIMS through the Laboratory for Innovative Key Materials and Structures (LINK *UMI 3629*), with additional contributions from Region Bretagne (France), and Fondation Langlois.

REFERENCES

[1] Saito, T; Imoto, H. Chalcogenide Cluster Complexes of Chromium, Molybdenum, Tungsten, and Rhenium. *Bull. Chem. Soc. Jpn.* **1996**, 69, 2403–2417.

[2] Yamagata, T.; Okiyama, H.; Imoto, H.; Saito, T. *trans*-[$(Mo_6Cl_8)(C_7H_7)_4\{P(n\text{-}C_4H_9)_3\}_2$] and *trans*-[$(Mo_6Cl_8)(C_8H_5)_4\{P(n\text{-}C_5H_{11})_3\}_2$].$2C_7H_8$. *Acta Cryst.* **1997**, C53, 859–862.

[3] Perrin, A.; Perrin, C. The Molybdenum and Rhenium Octahedral Cluster Chalcohalides in Solid State Chemistry: From Condensed to Discrete Cluster Units. *C. R. Chim.* **2012**, 15, 815–836.

[4] Abramov, P. A.; Rogachev, A. V.; Mikhailov, M. A.; Virovets, A. V.; Peresypkina, E. V.; Sokolov, M. N.; Fedin, V. P. Hexanuclear Chloride and Brimode Tungsten Clusters and Their Derivatives. *Russ. J. Coord. Chem.* **2014**, 40, 259–267.

[5] Cordier, S.; Grasset, F.; Molard, Y.; Amela-Cortes, M.; Boukherroub, R.; Ravaine, S.; Mortier, M.; Ohashi, N.; Saito, N.; Haneda, H. Inorganic Molybdenum Octahedral Nanosized Cluster Units, Versatile Functional Building Block for Nanoarchitectonics. *J. Inorg. Organomet. Polym. Mater.* **2015**, 25, 189–204.

[6] Vien, V.; Suh, M.-J.; Huh, S.; Kim, Y.; Kim, S.-J. Mesostructured Material Based on $[Re_6Te_8(CN)_6]^{4-}$ Cluster and Mn^{2+}: A Rational Synthesis of Hexagonal Nonoxidic Mesoscale Material. *Chem. Commun.* **2009**, 541–543.

[7] Kim, Y.; Fedorov, V. E.; Kim, S.-J. Novel Compounds Based on $[Re_6Q_8(L)_6]^{4-}$ (Q = S, Se, Te; L = CN, OH) and Their Applications. *J. Mater. Chem.* **2009**, 19, 7178–7190.

[8] Gray, T. G.; Rudzinski, C. M.; Meyer, E. E.; Holm, R. H.; Nocera, D. G. Spectroscopic and Photophysical Properties of Hexanuclear Rhenium(III) Chalcogenide Clusters. *J. Am. Chem. Soc.* **2003**, 125, 4755–4770.

[9] Kirakci, K.; Kubát, P.; Dušek, M.; Fejfarová, K.; Šícha, V.; Mosinger, J.; Lang, K. A Highly Luminescent Hexanuclear Molybdenum Cluster – A Promising Candidate toward Photoactive Materials. *Eur. J. Inorg. Chem.* **2012**, 19, 3107–3111.

[10] Kirakci, K.; Kubát, P.; Langmaier, J.; Polívka, T.; Fuciman, M.; Fejfarová, K.; Lang, K. A Comparative Study of the Redox and Excited State Properties of $(n\text{Bu}_4\text{N})_2[Mo_6X_{14}]$ and $(n\text{Bu}_4\text{N})_2[Mo_6X_8(CF_3COO)_6]$ (X = Cl, Br, or I). *Dalton Trans.* **2013**, 42, 7224–7232.

[11] Kirakci, K.; Fejfarová, K.; Kučeráková, M.; Lang, K. Hexamolybdenum Cluster Complexes with Pyrene and Anthracene Carboxylates: Ultrabright Red Emitters with the Antenna Effect. *Eur. J. Inorg. Chem.* **2014**, 14, 2331–2336.

[12] Saito, G.; Hosoda, H.; Yoshida, Y.; Hagiwara, J.; Nishimura, K.; Yamochi, H.; Otsuka, A.; Hiramatsu, T.; Shimazaki, Y.; Kirakci, K.; Cordier, S.; Perrin, C. Synthesis and Properties of Charge-Transfer Solids with Cluster Units $[Mo_6X_{14}]^{2-}$ (X = Br, I). *J. Mater. Chem.* **2012**, 22, 19774–19791.

[13] Chevrel, R.; Hirrien, M.; Sergent, M. Superconducting Chevrel Phases: Prospects and Perspectives. *Polyhedron* **1986**, 5, 87–94.

[14] Fischer, O.; Treyvaud, A.; Chevrel, R.; Sergent, M. Superconductivity in the $Re_xMo_6S_8$. *Solid State Commun.* **1975**, 17, 721–724.

[15] Maverick, A. W.; Gray, H. B. Luminescence and Redox Photochemistry of the Molybdenum(II) Cluster $Mo_6Cl_{14}^{2-}$. *J. Am. Chem. Soc.* **1981**, 103, 1298–1300.

[16] Gray, T. G.; Rudzinski, C. M.; Nocera, D. G.; Holm, R. H. Highly Emissive Hexanuclear Rhenium(III) Clusters Containing the Cubic Cores $[Re_6S_8]^{2+}$ and $[Re_6Se_8]^{2+}$. *Inorg. Chem.* **1999**, 38, 5932–5933.

[17] Zietlow, T. C.; Nocera, D. G.; Gray, H. B. Photophysics and Electrochemistry of Hexanuclear Tungsten Halide Clusters. *Inorg. Chem.* **1986**, 25, 1351–1353.

[18] Barras, A.; Cordier, S.; Boukherroub, R. Fast Photocatalytic Degradation of Rhodamine B over $[Mo_6Br_8(N_3)_6]^{2-}$ Cluster Units under Sun Light Irradiation. *Appl. Catal. B: Environ.* **2012**, 123–124, 1–8.

[19] Barras, A.; Das, M. R.; Devarapalli, R. R.; Shelke, M. V.; Cordier, S.; Szunerits, S.; Boukherroub, R. One-pot Synthesis of Gold Nanoparticle/Molybdenum Cluster/Graphene Oxide Nanocomposite and its Photocatalytic Activity. *Appl. Catal. B: Environ.* **2013**, 130–131, 270–276.

[20] Kumar, P.; Kumar, S.; Cordier, S.; Paofai, S.; Boukherroub, R.; Jain, S. L. Photoreduction of CO_2 to Methanol with Hexanuclear Molybdenum $[Mo_6Br_{14}]^{2-}$ Cluster Units under Visible Light Irradiation. *RSC Adv.* **2014**, 4, 10420–10423.

[21] Gray, H. B.; Maverick, A. W. Solar Chemistry of Metal Complexes. *Science* **1981**, 214, 1201–1205.

[22] Grasset, F.; Dorson, F.; Cordier, S.; Molard, Y.; Perrin, C.; Marie, A.-M.; Sasaki, T.; Haneda, H.; Bando, Y.; Mortier, M. Water-in-Oil Microemulsion Preparation and

Characterization of $Cs_2[Mo_6X_{14}]@SiO_2$ Phosphor Nanoparticles Based on Transition Metal Clusters (X = Cl, Br, and I). *Adv. Mater.* **2008**, 20, 143–148.

[23] Grasset, F.; Molard, Y.; Cordier, S.; Dorson, F.; Mortier, M.; Perrin, C.; Guilloux-Viry, M.; Sasaki, T.; Haneda, H. When "Metal Atom Clusters" Meet ZnO Nanocrystals: A $((n\text{-}C_4H_9)_4N)_2Mo_6Br_{14}$@ZnO Hybrid. *Adv. Mater.* **2008**, 20, 1710–1715.

[24] Grasset, F.; Dorson, F.; Molard, Y.; Cordier, S.; Demange, V.; Perrin, C.; Marchi-Artzner, V.; Haneda, H. One-pot Synthesis and Characterizations of Bi-functional Phosphor–Magnetic @SiO_2nanoparticles: Controlled and Structured Association of Mo_6 Cluster Units and γ-Fe_2O_3nanocrystals. *Chem. Commun.* **2008**, 39, 4729–4731.

[25] Cordier, S.; Dorson, F.; Grasset, F.; Molard, Y.; Fabre, B.; Haneda, H.; Sasaki, T.; Mortier, M.; Ababou-Girard, S.; Perrin, C. Novel Nanomaterials Based on Inorganic Molybdenum Octahedral Clusters. *J. Cluster Sci.* **2009**, 20, 9–21.

[26] Aubert, T.; Cabello-Hurtado, F.; Esnault, M.-A.; Neaime, C.; Lebret-Chauvel, D.; Jeanne, S.; Pallen, P.; Roiland, C.; Polles, L. L.; Saito, N.; Kimoto, K.; Haneda, H.; Ohashi, N.; Grasset, F.; Cordier, S. Extended Investigations on Luminescent $Cs_2[Mo_6Br_{14}]@SiO_2$ Nanoparticles: Physico-Structural Characterizations and Toxicity Studies. *J. Phys. Chem. C* **2013**, 117, 20154–20163.

[27] Truong, T. G.; Dierre, B.; Grasset, F.; Saito, N.; Saito, N.; Nguyen, T. KN.; Takahashi, K.; Uchikoshi, T.; Amela-Cortes, M.; Molard, Y.; Cordier, S.; Ohashi, N. Visible Tunable Lighting System Based on Polymer Composites Embedding ZnO and Metallic Clusters: From Colloids to Thin Films. *Sci. Technol. Adv. Mater.* **2016**, 17, 443–453.

[28] Maverick, A. W.; Najdzionek, J. S.; MacKenzie, D.; Nocera, D. G.; Gray, H. B. Spectroscopic, Electrochemical, and Photochemical Properties of Molybdenum(II) and Tungsten(II) Halide Clusters. *J. Am. Chem. Soc.* **1983**, 105, 1878–1882.

[29] Yoshimura, T.; Ishizaka, S.; Umakoshi, K.; Sasaki Y.; Kim, H.-B; Kitamura, N. Hexarhenium(III) Clusters $[Re_6(\mu_3\text{-}S)_8X_6]^{4-}$ (X^- = Cl^-, Br^-, I^-) are Luminescent at Room Temperature. *Chem. Lett.* **1999**, 28, 697–698.

[30] Mikhailov, M. A.; Brylev, K. A.; Abramov, P. A.; Sakuda, E.; Akagi, S.; Ito, A.; Kitamura, N.; Sokolov, M. N. Synthetic Tuning of Redox, Spectroscopic, and Photophysical Properties of $\{Mo_6I_8\}^{4+}$ Core Cluster Complexes by Terminal Carboxylate Ligands. *Inorg. Chem.* **2016**, 55, 8437−8445.

[31] Cotton, F. A.; Stanley, G. G. Ground State Electronic Structures of Some Metal Atom Cluster Compounds. *Chem. Phys. Lett.* **1978**, 58, 450–453.

[32] Honda, H.; Noro, T.; Tanaka, K.; Miyoshi, E. Theoretical Study on Electronic Excitation Spectra of Mo and Re Cluster Complexes: $[(Mo_6Cl_8)Cl_6]^{2-}$ and $[(Re_6S_8)Cl_6]^{4-}$. *J. Chem. Phys.* **2001**, 114, 10791–10797.

[33] Imoto, H.; Saito, T.; Adachi, H. Molecular Orbital Calculations of Octahedral Molybdenum Cluster Complexes with the DV-X.alpha. Method. *Inorg. Chem.* **1995**, 34, 2415–2422.

[34] Robinson, L. M.; Bain, R. L.; Shriver, D. F.; Ellis, D. E. Effect of Coordination Environment on the Electronic Structure and Properties of Mo_6-Based Systems: A Density Functional Treatment. *Inorg. Chem.* **1995**, 34, 5588–5596.

[35] Lin, Z.; Williams, I. D. Structure and Bonding in Face- and Edgebridged Octahedral Transition Metal Clusters. *Polyhedron* **1996**, 15, 3277–3287.

[36] Costuas, K.; Garreau, A.; Bulou, A.; Fontaine, B. ; Cuny, J.; Gautier, R.; Mortier, M.; Molard, Y.; Duvail, J.-L.; Faulques, E.; Cordier, S. Combined Theoretical and Time-Resolved Photoluminescence Investigations of $[Mo_6Br^i_8Br^a_6]^{2-}$ Metal Cluster Units: Evidence of Dual Emission. *Phys. Chem. Chem. Phys.* **2015**, 17, 28574–28585.

[37] Perdew, J. P.; Burke, K.; Ernzerhof, M. Generalized Gradient Approximation Made Simple. *Phys. Rev. Lett.* **1996**, 77, 3865–3868.

[38] Saito, N.; Wada, Y.; Lemoine, P.; Cordier, S.; Grasset, F.; Ohsawa, T.; Saito, N.; Cross, J.; Ohashi, N. Theoretical and Experimental Determination of the Crystal Structures of Cesium–Molybdenum Chloride. *Jpn. J. Appl. Phys.* **2016**, 55, 075502.

[39] Saito, N.; Lemoine, P.; Dumait, N.; Amela-Cortes, M.; Paofai, S.; Roisnel, T.; Nassif, V.; Grasset, F.; Wada, Y.; Ohashi, N.; Cordier, S. From $Cs_2Mo_6Cl_{14}$ to $Cs_2Mo_6Cl_{14}\cdot H_2O$ and Vice Versa: Crystal Chemistry Investigations. *J. Cluster Sci.* **2017**, DOI: 10.1007/s10876-016-1133-5.

[40] Kirackci, K.; Cordier, S.; Perrin, C. Synthesis and Characterization of $Cs_2Mo_6X_{14}$ (X = Br or I) Hexamolybdenum Cluster Halides: Efficient Mo_6 Cluster Precursors for Solution Chemistry Syntheses. *Z. Anorg. Allg. Chem.* **2005**, 631, 411–416.

[41] Shirley, D. A. High-Resolution X-Ray Photoemission Spectrum of the Valence Bands of Gold. *Phys. Rev. B* **1972**, 5, 4709–4714.

[42] Clark, S. J.; Segall, M. D.; Pickard, C. J.; Hasnip, P. J.; Probert, M. J.; Refson, K.; Payne, M. C. First Principles Methods Using CASTEP. *Z. Kristallogr.* **2005**, 220, 567–570.

[43] Milman, V.; Winkler, B.; White, J. A.; Pickard, C. J.; Payne, M. C.; Akhmatskaya, E. V.; Nobes, R. H. Electronic Structure, Properties, and Phase Stability of Inorganic Crystals: A Pseudopotential Plane-Wave Study. *Int. J. Quantum Chem.* **2000**, 77, 895–910.

[44] Hamann, D. R.; Schlüter, M.; Chiang, C. Norm-Conserving Pseudopotentials. *Phys. Rev. Lett.* **1979**, 43, 1494–1497.

[45] Hamann, D. R. Generalized Norm-Conserving Pseudopotentials. *Phys. Rev. B* **1989**, 40, 2980–2987.

[46] Rappe, A. W.; Rabe, K. M.; Kaxiras, E.; Joannopoulos, J. D. Optimized Pseudopotentials. *Phys. Rev. B* **1990**, 41, 1227–1230.

[47] Perdew, J. P.; Ruzsinszky, A.; Csonka, L. G. I.; Vydrov, O. A.; Scuseria, G. E.; Constantin, L. A.; Zhou, X.; Burke, K. Restoring the Density-Gradient Expansion for Exchange in Solids and Surfaces. *Phys. Rev. Lett.* **2008**, 100, 136406.

[48] Pulay, P. Convergence Acceleration of Iterative Sequences. The Case of SCF Iteration. *Chem. Phys. Lett.* **1980**, 73, 393–397.

[49] Pfrommer, B. G.; Côté, M.; Louie, S. G.; Cohen, M. L. Relaxation of Crystals with the Quasi-Newton Method. *J. Comput. Phys.* **1997**, 131, 233–240.

[50] Monkhorst, H. J.; Pack, J. D. Special Points for Brillouin-Zone Integrations. *Phys. Rev. B* **1976**, 13, 5188–5192.

[51] Pack, J. D.; Monkhorst, H. J. "Special Points for Brillouin-Zone Integrations"—A Reply. *Phys. Rev. B* **1977**, 15, 1748–1749.

[52] Segall, M. D.; Shah, R.; Pickard, C. J.; Payne, M. C. Population Analysis of Plane-Wave Electronic Structure Calculations of Bulk Materials. *Phys. Rev. B* **1996**, 54, 16317–16320.

[53] Segall, M. D.; Lindan, P. J. D.; Probert, M. J.; Pickard, C. J.; Hasnip, P. J.; Clark, S. J.; Payne, M. C. First-Principles Simulation: Ideas, Illustrations and the CASTEP Code. *J. Phys.: Condens. Matter* **2002**, 14, 2717–2744.

[54] Hirshfeld, F. L. Bonded-Atom Fragments for Describing Molecular Charge Densities. *Theor. Chim. Acta* **1977**, 44, 129–138.

[55] Wiberg, K. B.; Rablen, P. R. Comparison of Atomic Charges Derived via Different Procedures. *J. Comput. Chem.* **1993**, 14, 1504–1518.

[56] Scofield, J. H. Hartree-Slater Subshell Photoionization Cross-Sections at 1254 and 1487 eV. *J. Electron Spectrosc. Relat. Phenom.* **1976**, 8, 129–137.

[57] Haas, P.; Tran, F.; Blaha, P. Calculation of the Lattice Constant of Solids with Semilocal Functionals. *Phys. Rev. B* **2009**, 79, 085104.

[58] Sanchez-Portal, D.; Artacho, E.; Soler, J. M. Projection of Plane-Wave Calculations into Atomic Orbitals. *Solid State Commun.* **1995**, 95, 685–690.

[59] Wendlandt, W. W.; Hecht, H. G. *Reflectance Spectroscopy*; Interscience Pub.: New York, 1966.

[60] Tandon, S. P.; Gupta, J. P. Measurement of Forbidden Energy Gap of Semiconductors by Diffuse Reflectance Technique. *Phys. Stat. Sol.* **1970**, 38, 363–367.

[61] Perdew, J. P.; Zunger, A. Self-Interaction Correction to Density-Functional Approximations for Many-Electron Systems. *Phys. Rev. B* **1981**, 23, 5048–5079.

[62] Heyd, J.; Peralta, J. E.; Scuseria, G. E.; Martin, R. L. Energy Band Gaps and Lattice Parameters Evaluated with the Heyd-Scuseria-Ernzerhof Screened Hybrid Functional. *J. Chem. Phys.* **2005**, 123, 174101.

[63] Ramirez-Tagle, R.; Arratia-Pérez, R. Electronic Structure and Molecular Properties of the $[Mo_6X_8L_6]^{2-}$; X = Cl, Br, I; L = F, Cl, Br, I Clusters. *Chem. Phys. Lett.* **2008**, 460, 438–441.

[64] Hamer, A. D.; Walton, R. A. X-Ray Photoelectron Spectra of Inorganic Molecules. IX. Distinction Between Bridging and Terminal Metal-Chlorine Bonds in Metal Halide Clusters of Rhenium(III) and Molybdenum(II). *Inorg. Chem.* **1974**, 13, 1446–1451.

[65] Walton, R. A. Some Recent Aspects of the X-Ray Photoelectron Spectra and Chemistry of Low Oxidation State Molybdenum Halides and Their Complexes. *J. Less-Common Met.* **1977**, 54, 71–80.

[66] Best, S. A.; Walton, R. A. X-Ray Photoelectron Spectra of Inorganic Molecules. 22. Halogen Core Electron Binding Energies of Low Oxidation State Molybdenum Bromide and Molybdenum Iodide Clusters and Niobium and Tantalum Chlorides Containing the $[M_6Cl_{12}]^{n+}$ Cores. *Inorg. Chem.* **1979**, 18, 484–488.

[67] Preetz, W.; Harder, K.; Von Schnering, H. G.; Kliche, G.; Peters, K. Synthesis, Structure and Properties of the Cluster Anions $[(Mo_6Cl^i_8)X^a_6]^{2-}$ with $X^a \equiv$ F, C1, Br, I*. *J. Alloys Compd.* **1992**, 183, 413–429.

[68] Preetz, W.; Bublitz, D.; Von Schnering, H. G.; Saßmannshausen, J. Darstellung, KriDarstellung, Kristallstruktur und spektroskopische Eigenschaften der Clusteranionen $[(Mo_6Br^i_8)X^a_6]^{2-}$ mit X^a = F, Cl, Br, I. *Z. Anorg. Allg. Chem.* **1994**, 620, 234–246.

For Table of Contents Only

The electronic and crystal structures of $Cs_2[Mo_6X_{14}]$ (X = Cl, Br, I) ternary cluster-based compounds were investigated by density functional theory (DFT) simulations and experimental methods. The experimentally refined lattice parameters were in good agreement with theoretical optimized ones. The calculated band gaps also reproduced those photo-spectroscopically determined within an error of a few eV. The X-ray photoemission valence spectra were fairly reproduced from projected density of state (PDOS) weighted with cross-sections of Al K_α.

Table of Contents graphic

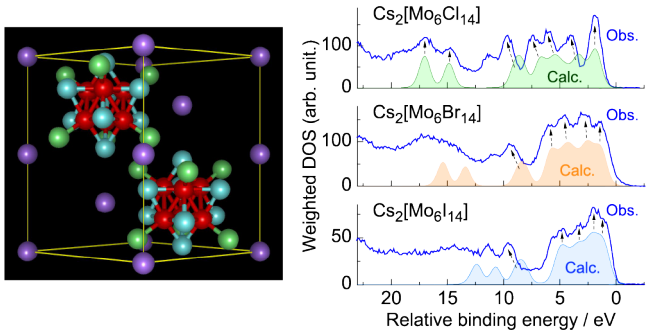

For Table of Contents Only